J. Electroanal. Chem., 339 (1992) 423–449
Elsevier Sequoia S.A., Lausanne
JEC 02186

The application of fast scan cyclic voltammetry. Mechanistic study of the initial stage of electropolymerization of aniline in aqueous solutions *

Hongjun Yang and Allen J. Bard

Department of Chemistry and Biochemistry, The University of Texas at Austin, Austin, TX 78712 (USA)

(Received 18 February 1992; in revised form 22 April 1992)

Abstract

The initial stage of electropolymerization of aniline in acidic aqueous solution was studied by cyclic voltammetry and digital simulation. The dimer of aniline, *p*-aminodiphenylamine (ADPA), is the dominant intermediate in the early stages of polymerization, while benzidine is a minor intermediate. Cyclic voltammetric studies at a glassy carbon electrode in aniline solutions of low concentration combined with digital simulation indicated that both intermediates, benzidine and *p*-aminodiphenylamine, are formed through radical-cation–radical-cation coupling pathways. The reduction wave for the aniline radical cation was observed for the first time by working at a low aniline concentration (0.05 mM) and at a scan rate of 200 V s^{-1}. The rate constant for the dimerization of aniline radical cations is about 10^8 M^{-1} s^{-1}.

Because of kinetic control of electropolymerization of aniline, the polymer morphology depended upon scan rate. Scanning electron and scanning tunneling microscopic images of the polyaniline films formed showed that the films produced at fast scan rates were more uniform, compact, and of a more regular structure than those produced at slow scan rates.

INTRODUCTION

We discuss the application of voltammetry to a study of the kinetics and mechanism of the initial stage in the electropolymerization of aniline in aqueous solutions. Polyaniline (PANI), an electronically conducting polymer, has been of interest over the past decade [1–10]. During the 1980s, the structural, physical, and

* Dedicated to Professor Ernest Yeager on the occasion of his retirement and in recognition of his contribution to electrochemistry.

electrical properties of polyaniline were characterized by a number of experimental techniques. Electrochemical methods, frequently used to polymerize aniline, are also used to obtain information on the mechanism of polymer growth, as well as the redox behavior and mode of electronic conduction of PANI.

Recently, several groups have proposed an autocatalytic mechanism for polyaniline growth [11–22]. After the initiation step, PANI grows without oxidation of aniline, i.e. at the potential for oxidation of PANI, which is less positive than that of the monomer, aniline. The oxidized PANI presumably incorporates monomeric aniline at its chain end and the resultant chain is again oxidized electrochemically to incorporate another monomer aniline from the solution phase. Stilwell and Park [11] reported that the growth rate was first order in aniline concentration; at longer oxidation times during growth, side reactions play more important roles compared with the earlier phase of the growth process.

The mechanism for oxidation and reduction of PANI is important in understanding the polymer growth, conduction, and degradation mechanisms. MacDiarmid and coworkers [19–21,23,24] studied the electrochemical oxidation of PANI and reduction of the oxidized (doped) form in aqueous electrolytes of different pH values. They propose that at different potentials two classes of redox processes occur that differ from each other by the extent to which the processes are accompanied by deprotonation (during oxidation) and protonation (during reduction).

Conduction of organic polymers occurs via polarons (radical cation states) and bipolarons (dicationic states). When diradical dications are generated, further polyaniline growth can occur, if aniline is present in the solution, a degradation reaction via hydrolysis is also possible. Overoxidation may also cause cross-linkage of the linear polymers to form a three-dimensional polymer structure.

The above mentioned mechanisms are commonly accepted. The actual overall reaction mechanisms are probably even more complicated. For example, all of the proposed mechanisms are based on the assumption that the initial dimerization product is a "head-to-tail" dimer, *p*-aminodiphenylamine (ADPA). However, the "tail-to-tail" dimer, benzidine, also forms and can participate in the polymerization reaction, as suggested in a recent report [25], where a conductive polybenzidine film was formed electrochemically. The important, unresolved, question concerning the mechanism of the initial oxidation and dimerization reactions of aniline still remains. Investigation of the mechanism of the initial dimerization is difficult, because the lifetime of cation radical generated upon oxidation of aniline is very short and it is difficult to detect. For example, Genies and Lapkowski reported that no electron spin resonance signal was observed during the oxidation of aniline [16].

We recently reported investigations of the initial stage of the oxidation and dimerization of diphenylamine and *N*,*N*-dimethylaniline in MeCN by fast scan cyclic voltammetry with ultramicroelectrodes [26,27]. In the present study, we extend this work to the initial stage of the oxidation and dimerization of aniline in aqueous solutions.

EXPERIMENTAL

The electrochemical cell and instrumentation for voltammetry have been described previously [26–28]. In aqueous solutions, a saturated mercurous sulfate electrode (SMSE) was used as the reference electrode. Aniline (J.T. Baker Inc., Phillipsburg, NJ) was distilled twice over zinc powder on a vacuum line and kept under argon. Sulfuric acid (Fisher Scientific Company, Fair Lawn, NJ) was used as received. Water was Millipore milli-Q grade. *p*-Aminodiphenylamine (ADPA) (Aldrich Chemical Company, Inc., Milwaukee, WI) was dissolved in ethanol and filtered to remove insoluble impurities and then recrystallized from cyclohexane. Because of the low solubility of ADPA in H_2SO_4 solution, a small amount of MeCN (about 4% by volume) was added to the H_2SO_4 solution in the electrochemical study. All other chemicals were reagent grade and were used as received.

The platinum electrodes used as scanning tunneling microscopy (STM) substrates were made by sputtering platinum at approximately 10^{-6} Torr onto the exposed area (1 or 2 mm diameter circular spots) on a glass slide.

Digital simulation was performed on an IBM/PS2-30286 equipped with a 80287 math coprocessor. Microsoft Fortran 5.0 was used for compiling.

RESULTS

Cyclic voltammetry

For purposes of orientation, a typical cyclic voltammogram at scan rate v of 100 mV s^{-1} taken during the oxidation of aniline and polyaniline film growth is shown in Fig. 1. This voltammogram is very similar to that reported by Stilwell and Park [11] and analyzed and discussed by them. The multiple redox waves indicate the complexity of the electro-oxidation of aniline which involves coupled multiple heterogeneous electron transfer reactions and homogeneous chemical reactions. The different waves and the processes ascribed to these are summarized in Table 1. The broad anodic peak E on the first scan at 0.62 V corresponds to the oxidation of aniline. As cycling continued, this peak height decreased and finally essentially disappeared. At more negative potentials, four pairs of well defined peaks gradually formed. These become better defined and the current on the cathodic and anodic waves increased with time. The increasing current with each cycle reflects the growth of the polymer film. Peak A apparently has the characteristics of a surface wave and has been identified as the oxidation of the reduced form of PANI to the radical cation (polaron) state. Peak A′ is broad with a potential about 120 mV negative of that of peak A and corresponds to the reduction of different states of oxidized PANI to the fully reduced form. Peak D is assigned to the oxidation of the polymer to form the dication or diradical dication state of the polymer and D′ to the reduction of these [11,13,16]. Note that in the later stages of polymer growth, after about 5 min cycling, peaks B and B′ and C and C′ grew and became more pronounced; these have been attributed to the

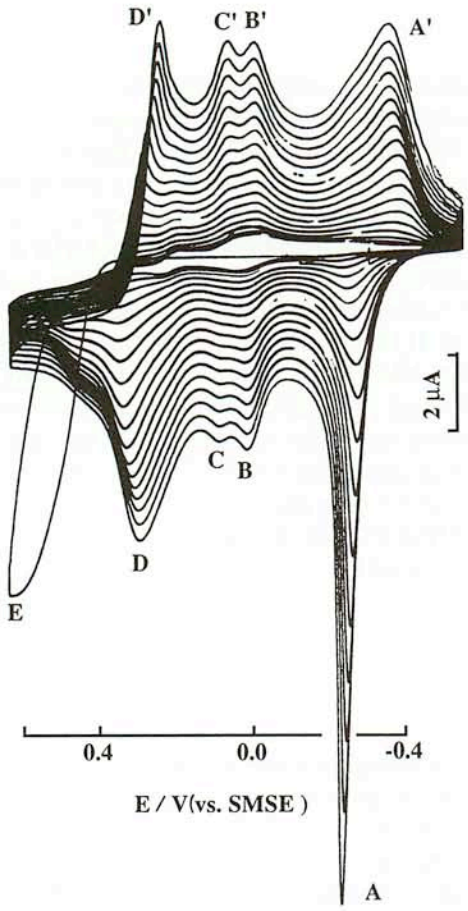

Fig. 1. Cyclic voltammogram of 20 mM aniline in 1 M H_2SO_4 solution with 0.5 mm diameter platinum disk electrode at a scan rate of 0.1 V s^{-1} after 10 min.

TABLE 1

Summary of cyclic voltammetry waves

	Assigned species	$E_{1/2}$ /V vs. SMSE
A/A′	Polaron states of PANI (0/+1)	≈ −0.3
B/B′	Benzoquinone/hydroquinone(BQ/HQ)	≈ −0.02
C/C′	*p*-aminophenol/benzoquinoneimine	≈ 0.08
D/D′	Bipolaron states of PANI (+1/+2)	≈ 0.27
E	Oxidation of aniline	E_{pa} = 0.62
F/F′	Benzidine (0/+2)	0.23
G/G′	ADPA (0/+2)	−0.02
H/H′	*p*-hydroxydiphenylamine (0/+2)	0.08
I	Unknown	E_{pa} = 0.50

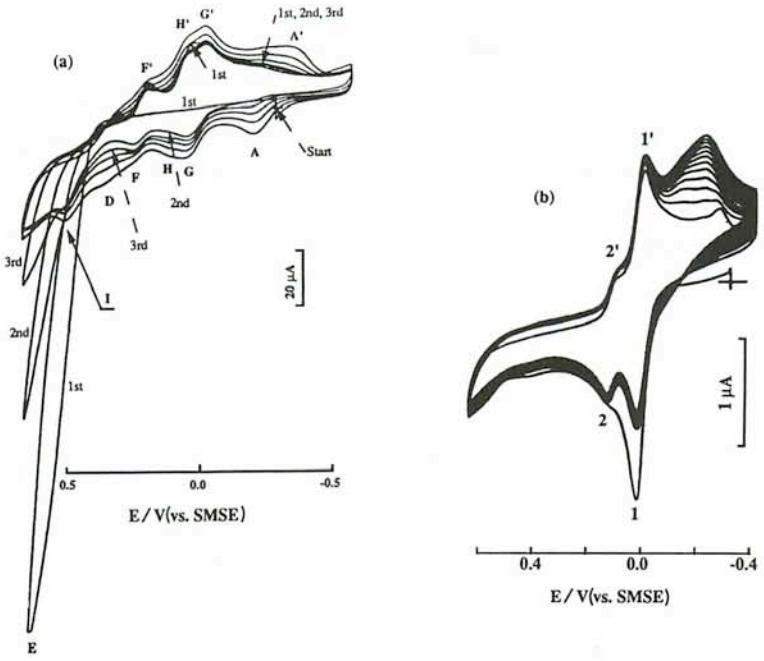

Fig. 2. (a) Cyclic voltammogram of 20 mM aniline in 1 M H_2SO_4 solution with 2 mm diameter platinum disk electrode at a scan rate of 0.05 V s^{-1}. (b) Cyclic voltammogram of 0.8 mM 4-aminodiphenylamine in 1 M H_2SO_4 solution with 0.5 mm diameter platinum disk electrode at a scan rate of 0.1 V s^{-1}.

oxidation and reduction of degradation products, *p*-benzoquinone/hydroquinone and *p*-aminophenol [11,13].

Our interest is in the early stages of PANI film growth. Figure 2(a) shows the first six cycles of the cyclic voltammogram at 50 mV s^{-1}. At least two or more pairs of peaks appear. Special attention should be directed to the first two cycles. Upon oxidation of the aniline monomer, four peaks appear on the cathodic branch, and five peaks are observed on the following positive scan. At this stage, there is no evident wave for D/D′, but the wave for A/A′ is present. This suggests that the polymer skeleton has not yet formed. The species responsible for peaks F/F′ has been identified as the tail-to-tail dimeric intermediate, benzidine, by an in situ spectroelectrochemical method [11]. We designate the other pairs of peaks as G/G′ and H/H′ to distinguish them from B/B′ and C/C′ formed at a later stage and shown in Fig. 1. Although the potentials of G/G′ and H/H′ are almost the same as those for B/B′ and C/C′, they represent different processes. In the earliest stage of polymerization, the cation radicals generated by electro-oxidation of aniline couple by head-to-tail and tail-to-tail dimerization to form *p*-aminodiphenylamine (ADPA) and benzidine respectively [4]. The dimerization associated with deprotonation is the dominant reaction. Either G/G′ or H/H′ can be identified with ADPA redox processes, as reported by Hand and Nelson [29] and

Stilwell and Park [11]. Dimer ADPA in acidic aqueous solution can undergo an oxidative decomposition reaction, ultimately leading to hydrolysis to form *p*-hydroxydiphenylamine, which is a relatively slow step [11,29]. This species, *p*-hydroxydiphenylamine, can be further oxidized to generate the quinoneimine that then cleaves to form benzoquinone and anilinium. Therefore, a successive ECE-CEC process would occur, starting with the oxidation of ADPA.

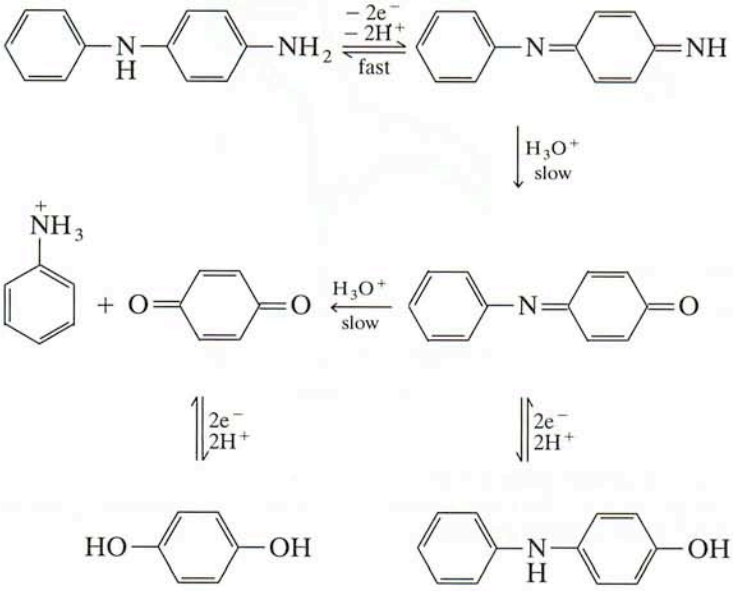

The potentials for all of these electron transfers are very near one another, so that peaks G and H, G′ and H′ merge to form broader waves beginning with the second cycle.

Figure 2(b) shows the cyclic voltammogram of ADPA in 1 M H_2SO_4. In the first positive scan, at more positive potentials than that of the oxidation of ADPA, a small electrochemically reversible wave appeared, 2 and 2′. This is due to a kinetically slow step for the oxidative decomposition reaction of ADPA [11,29]. In the following cycles, peak 2 reaches a steady state, which suggests that the hydrolysis reaction reaches equilibrium. Note that the peak potentials of 1/1′ and 2/2′ are the same as those of G/G′ and H/H′ in Fig. 2(a). Therefore, it is reasonable to designate G/G′ as the redox couple of the head-to-tail dimer, ADPA, and peaks H/H′ as that of *p*-hydroxydiphenylamine.

Peaks F and F′ have been associated with benzidine redox processes, by comparison with cyclic voltammetry of an authentic sample [13]. Note that the cathodic current peaks G′ and H′ are higher than peak F′ during the first cycle in Fig. 2(a), which indicates that the two alternative dimerization reactions yield different quantities of head-to-tail dimer and tail-to-tail dimer; this implies that the coupling reactions have different rates, as discussed below. Since the solubility of ADPA is limited in H_2SO_4, some ADPA deposited onto the electrode surface

causes an increase in the *IR* drop at the electrode surface. The peak currents of F′, G′, and H′ decreased slightly during the second cycle. As conductive PANI formed and grew, all of these currents increased again because of an effective increase in electrode area. Note also in Fig. 2(a) that as peak E decreased and finally disappeared, peaks F/F′ also became smaller and eventually vanished. This suggests that the formation of benzidine depends strongly upon the oxidation of aniline, i.e. on aniline cation radicals, rather than on aniline itself. This behavior is similar to that seen with diphenylamine [26] and *N*,*N*-dimethylaniline [27] in MeCN. Peaks G/G′ and H/H′ grew during continued scanning because the series ECEC processes (autocatalytic reaction) took place.

Figure 2(a) also shows the quenching effect discussed by Stilwell and Park [11]. Note that before peak D appeared, e.g. in the 2nd to 4th cycles, there was a peak I located about 100 mV more positive than peak D. Although we were not able to identify the intermediate giving rise to this peak, it is probably a highly oxidized state of an oligomer. This oxidized state of the intermediate has the same fate as that of peak D, which appeared later. In the presence of aniline, it reacts with another molecule of aniline behaving as a nucleophile. Such a nucleophilic addition increases the length of the oligomer. Thus, the backwaves I′, and later D′, decreased. This effect is important in the earlier stages of polymer growth. One can see that peak D grows relatively rapidly, so that peak I ultimately merges with it (Fig. 1). In the later stages of PANI growth, the quenching effect became less important. Compared with Fig. 2(a), peak D′ in Fig. 1 is more pronounced and sharper during the later stage of PANI growth. Associated with the quenching effect, a cross-over current was shown at the beginning of the first negative scan (Fig. 2(a)). This behavior has been attributed to nucleation of polymer molecules [30].

As mentioned above, the anodic peak A is regarded as the appearance of a polaron state [9–11,16], which is transformed into a bipolaron state at the potential of peak D. The mechanism of redox transfer of the bipolaron in a PANI film is reported to be very different from that of the polaron [16]. The in situ ESR signal for the bipolaron was much smaller than that of the polaron. Note that peak A appears much earlier than peak D during PANI growth. Peak D does not appear until after five potential cycles (Fig. 2(a)), while peak A is observed clearly in the early cycles.

The complex nature of the redox reactions during PANI growth is clearly shown in the cyclic voltammograms in Figs. 1 and 2(a). Two parallel sets of reactions occur, polymer growth and degradation. In the earlier stage, polymer growth predominates. Dimerization and nucleophilic addition are the dominant reactions. As the polymer backbone builds up, the charges on the oxidized PANI become delocalized. Thus, the driving force for aniline nucleophilic addition becomes weaker. Simultaneously, water, another nucleophile in the system, probably attacks the oxidized PANI in a nucleophilic hydrolysis reaction. When this occurs, degradation becomes important.

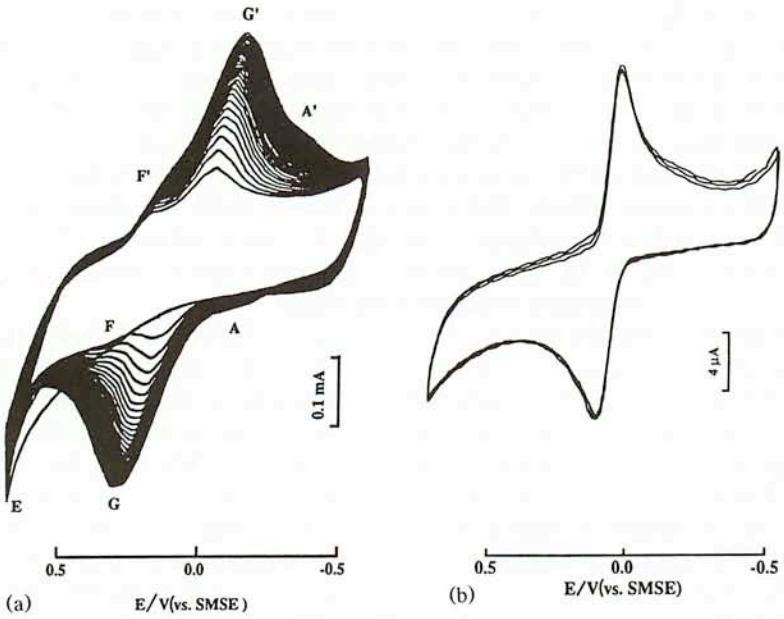

Fig. 3. (a) Cyclic voltammogram of 20 mM aniline in 1 M H_2SO_4 solution with 1 mm diameter platinum disk electrode at a scan rate of 20 V s^{-1}. (b) Cyclic voltammogram of 1.67 mM 4-aminodiphenylamine in 1 M H_2SO_4 solution with 0.5 mm diameter platinum disk electrode at a scan rate of 10 V s^{-1}.

Kinetic control of the early stages of PANI growth

The cyclic voltammetry behavior is different at faster scan rates. Figure 3(a) shows the cyclic voltammogram of the same system as in Figs. 1 and 2(a) with a 1 mm diameter platinum electrode at $v = 20$ V s^{-1}. The fast-scan voltammogram shows fewer waves. After anodic oxidation of aniline at 0.62 V, only two cathodic peaks F′ and G′ appear on the first reversal. In the following cycles, the growth of peaks F/F′ and G/G′ are clearly observed. A noticeable feature of this voltammogram is the absence of peaks H/H′. As described above, peaks H/H′ are attributed to the *p*-hydroxydiphenylamine/quinoneimine couple. The absence of these suggests that a kinetically slow oxidative hydrolysis starting from ADPA did not occur during the fast potential scan. Consequently, the follow-up series of EC steps is also absent.

A number of cyclic voltammograms with different concentrations of ADPA in 1 M H_2SO_4 solution at various scan rates were obtained. At 10 V s^{-1} the oxidation of ADPA is chemically reversible (Fig. 3(b)). For all ADPA concentrations examined (0.5–5 mM), waves 2/2′, seen in Fig. 2(b), decreased in size with an increase in scan rate and disappeared above 10 V s^{-1}. Therefore, we conclude that the oxidative hydrolysis of ADPA is relatively slow. Since the reversible redox behavior of ADPA at 10 V s^{-1} was not affected by a change in ADPA concentra-

tion, the hydrolysis of the quinonediimine appears to be pseudo first order. Thus, if the kinetic parameter, $\lambda = (k/v)(RT/nF) \ll 0.1$, i.e. the system is assumed to be in the DP (pure diffusion) zone [31], the magnitude of the rate constant for hydrolysis is estimated as less than 10 s^{-1}. This kinetic analysis of the oxidative hydrolysis reaction of APDA thus accounts for the absence of peaks H/H′ in Fig. 3(a). This also suggests that the polymerization of aniline can be controlled kinetically, by a change in scan rates.

The growth of the peak currents of G/G′ is faster than that of F/F′ in Fig. 3(a). Although the curves in Fig. 2(a) show that the rate of formation of benzidine and ADPA are not equal during the early stages, the oxidative hydrolysis of ADPA and later degradation of PANI made it difficult to examine closely the peak currents for these two dimers. Here, the fast growth of peak currents G/G′ for ADPA over that for benzidine F/F′ is clearly seen in Fig. 3(a). This supports the assertion that the two couplings have different rates, with the dimerization resulting in the head-to-tail dimer faster than that for the tail-to-tail dimer, benzidine. This suggests that kinetic control of PANI growth is possible.

Figures 4(a)–4(c) are the cyclic voltammograms at 500 V s^{-1} obtained with a 50 μm diameter platinum microelectrode and recorded for 1–30 cycles, 61–90 cycles, and 271–300 cycles respectively. At this scan rate, the formation of benzidine was completely suppressed. The initial dimer product was ADPA. With continued scanning, the waves responsible for the redox reaction of ADPA grew in quickly and, because of partial solubility of ADPA, have surface wave characteristics. Note that the anodic current E for the oxidation of aniline decreased while peaks G/G′ grew, implying that PANI growth at high scan rates is based on the oxidation of the dimer, ADPA, and oligomers with monomer addition. The waves corresponding to the formation of the polaron state appear earlier than those of the bipolaron state. This is the usual behavior in PANI growth whatever the scan rate (Figs. 2(a), 3(a), 4). We speculate that the polaron state can form in the oligomer, but the bipolaron state only exists in the well structured polymer. The PANI formed at this scan rate should presumbly possess better properties, because this ADPA-based PANI has a more regular chain structure, as described in the introduction. This suggests a unique advantage for the ADPA-based PANI formed at high scan rates.

Cyclic voltammetry with different concentrations of aniline at high scan rates was also carried out to determine the time scale at which the benzidine waves disappeared. This depended on the bulk concentration of aniline. The higher the concentration, the shorter the time scale, as expected for a second-order dimerization reaction. These results led to an estimate of the rate constant for this dimerization reaction as greater than 10^6 M^{-1} s^{-1}.

Morphology of PANI films

We recently reported the use of scanning electron microscopy (SEM) and scanning tunneling microscopy (STM) to reveal the morphologies of thin PANI films formed by cyclic voltammetry at different scan rates [28]. For completeness, a

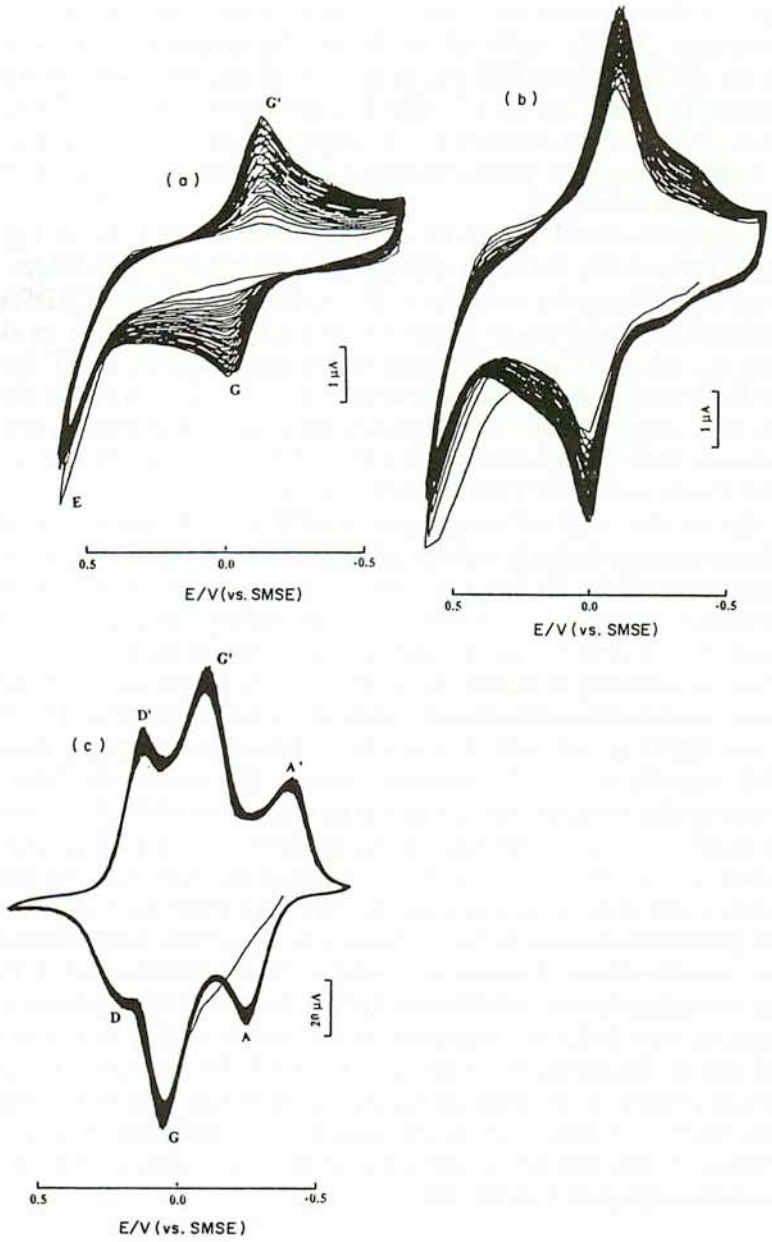

Fig. 4. Cyclic voltammograms of 20 mM aniline in 1 M H_2SO_4 solution with 25 mm diameter platinum microdisk electrode at a scan rate of 500 V s^{-1}; (a) 1–30, (b) 61–90, (c) 271–300 cycles.

brief discussion of high resolution microscopic images is given here as well. STM is especially useful for examining thin film (less than 500 Å) structures with high resolution. For PANI formed in the early stages (six cycles) of growth at slow scan

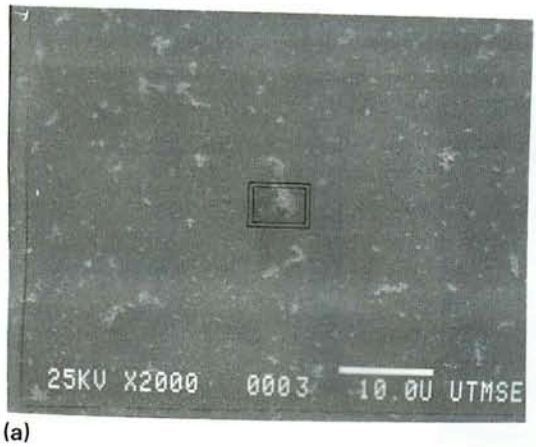

(a)

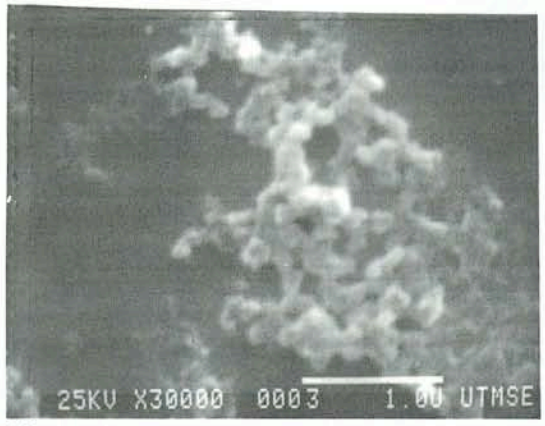

(b)

Fig. 5. (a) SEM image of the PANI film prepared in Fig. 2(a). (b) An enlarged image of (a).

rate, 50 mV s^{-1}, i.e. as in Fig. 2(a), the SEM images show only a few aggregates (Fig. 5(a)). Closer examination of the aggregate, Fig. 5(b), did not reveal clear features and the STM image shows that the surface structure is rather amorphous, although a microfiber structure could occasionally be seen [28]. The STM image of PANI obtained at 20 V s^{-1} is more interesting (Fig. 6). A film deposited onto a platinum electrode by passing the same total anodic charge (approximately 35 mC cm^{-2}) as that at slow scan rate, appears as particles of uniform size composed of chain bundles. These bundles seemed to be oriented at various angles with respect to the substrate.

A sample PANI film prepared under the same high scan rate conditions used in Fig. 6 was also examined by SEM. The SEM image at the same resolution as that in Fig. 5 failed to resolve any of the distinct features in Fig. 6 and showed only a flat uniform surface [28]. This clearly differentiates the resolution of STM and

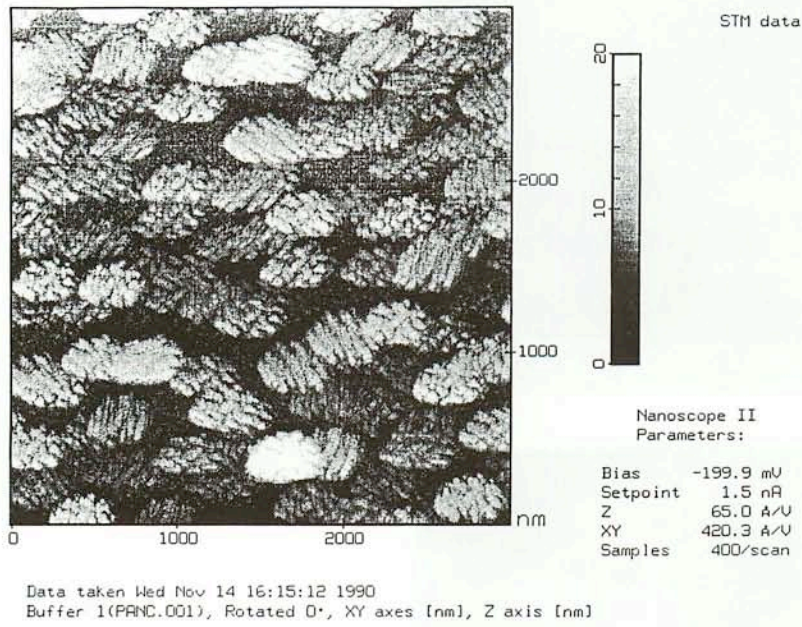

Fig. 6. STM image of the PANI film prepared in Fig. 3(a).

SEM; for thin films (approximately 100 Å), STM can provide greater structural information.

In the later stage of PANI growth, the polymer film became thicker (greater than 1 μm) and STM was less informative. Figure 7 shows SEM images of the morphology of a PANI film deposited onto a 100 μm diameter platinum disk from a 20 mM aniline solution at 0.05 V s^{-1} by passing a total anodic charge of about 0.3 C cm^{-2}. The microfiber structure can be seen clearly. SEM images obtained with 50 μm platinum at a scan rate of 500 V s^{-1} by passing a total anodic charge of about 0.1 C cm^{-2} showed a thin, compact and uniform PANI film (Fig. 8). No microfiber structure was observed. The STM and SEM results show that PANI films formed at slow scan rates are very different from those produced at fast scan rates. The differences arise from different reactions in the polymerization–degradation pathways that are important at the different time scales. Presumably the reactions involving benzidine and degradation products are less important at rapid scan rates.

Radical–radical coupling vs. radical–parent coupling

Upon anodic oxidation of aniline at a platinum electrode surface in aqueous acidic solution, ADPA and benzidine are the major dimerization products, while hydrolysis occurs with the oxidized APDA. The proportion of the tail-to-tail and

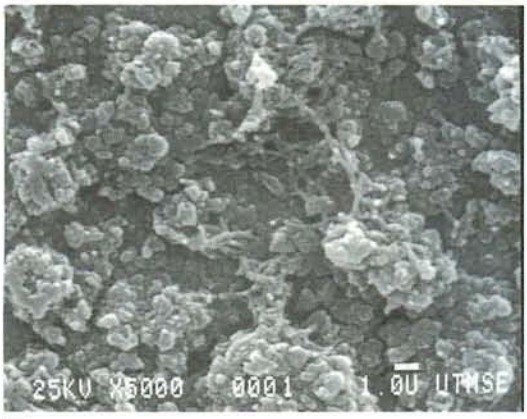

(a)

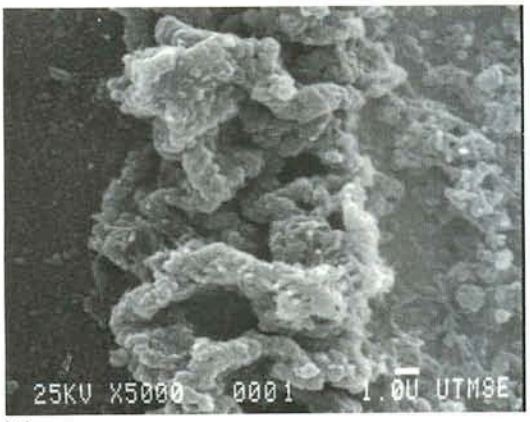

(b)

Fig. 7. SEM images of PANI film prepared in 20 mM aniline, 1 M H_2SO_4 solution with 100 μm diameter platinum disk at a scan rate of 0.05 V s^{-1} by passing a total anodic charge of 0.3 C cm^{-2} (a) in the center, and (b) at the edge of the electrode.

head-to-tail coupling products indicates different rates for these two pathways as already discussed.

Because of the fast rates and complex mechanisms of the homogeneous reactions following the initial electron transfer to form the aniline radical cation, a mechanistic study of the coupling pathways in detail is difficult. Ultimately our main aim was to determine whether the dimerization proceeds through radical–radical (R–R) or radical–parent monomer (R–P) coupling. Gao et al. [32] recently suggested that for aniline adsorbed on a gold electrode surface, radical cations should favor a tail-to-tail coupling to yield exclusively benzidine, based on SERS studies. They also suggested that the formation of the "head-to-tail" product, ADPA, can be understood in terms of coupling between the radical cation and

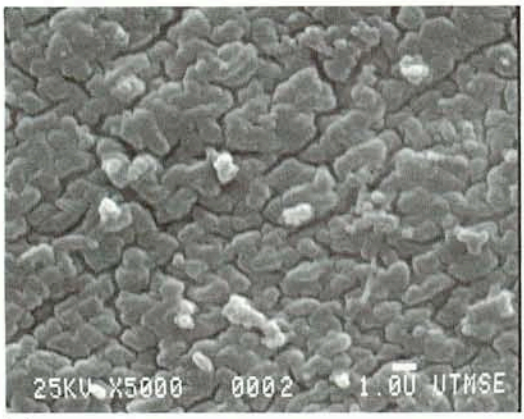

(a)

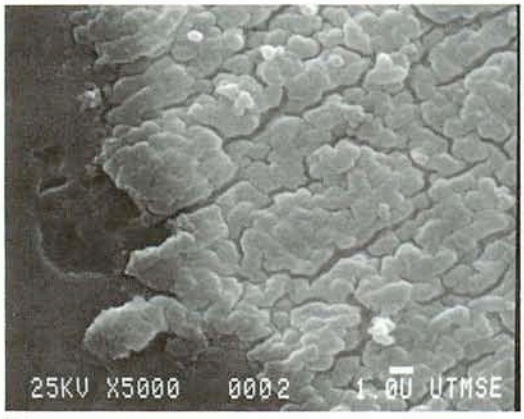

(b)

Fig. 8. SEM images of PANI film prepared in 20 mM aniline 1 M H_2SO_4 solution with 50 μm diameter platinum disk at a scan rate of 500 V s^{-1} by passing a total anodic charge of 0.1 C cm^{-2} (a) in the center, and (b) at the edge of the electrode.

parent molecule, although the possibility of R–R coupling to produce ADPA still exists.

To study the initial stage of the oxidation of aniline, lower aniline concentrations are desirable to decrease the rates of the dimerization reactions. However, when the aniline concentration was below 5 mM, oxide formation and reduction on platinum in sulfuric acid interfered in the voltammogram of aniline. To avoid this, a glassy carbon (GC) electrode was used in voltammetric measurements. Figure 9 is a cyclic voltammogram of 1 mM aniline in 1 M H_2SO_4 at a GC electrode, which is slightly different from that at platinum for the same value of v. No peaks for the oxidative hydrolysis product appeared to interfere with the redox behavior of ADPA. The peak potential separations ΔE_p for the redox couples, benzidine and

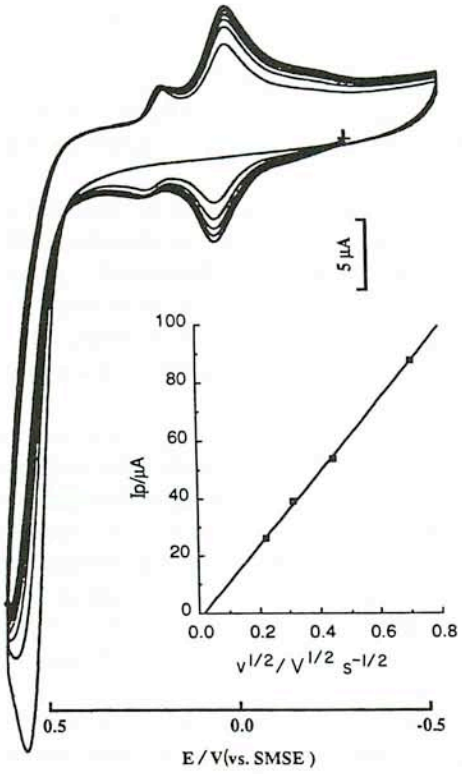

Fig. 9. Cyclic voltammogram of 1 mM aniline in 1 M H_2SO_4 solution with 3 mm diameter glassy carbon electrode at a scan rate of 0.1 V s^{-1}.

ADPA, are both 30 mV, which suggests that two electrons are involved in the redox processes of both species [31]. The potential difference between the first oxidation peak of aniline and its half peak was 40 mV for v from 0.05 to 0.5 V s^{-1}. However, the E_p for the first oxidation wave shifted about 20 mV toward more positive potentials as v increased from 0.05 to 0.5 V s^{-1}. At these scan rates, I_p for aniline oxidation during the first scan was proportional to $v^{1/2}$, indicating that the reaction was diffusion controlled.

The ratio of I_{pa} for the first wave to I_{pc} for benzidine and for ADPA on the first reversal is about 11 : 0.64 : 1, correcting for base lines. This proportion provides a rough estimate of the relative rate constants for the coupling reactions.

To elucidate the mechanism of the coupling pathway, digital simulations were carried out and compared with the experimental cyclic voltammograms [26,27]. Four mechanisms were considered.

(1) Both benzidine and ADPA were formed by R–R coupling (denoted R–R).

(2) Benzidine was formed by R–R coupling while ADPA was formed by R–P coupling (denoted R–P1).

(3) Benzidine was formed by R–P coupling while ADPA was formed by R–R coupling (denoted R–P1′).
(4) Both compounds were formed by R–P coupling (denoted R–P2).

For R–P coupling, it was assumed that the coupling product would lose another electron. Thus, the total number of electrons transferred in overall reactions would be the same in all of the simulated mechanisms.

The simulation was difficult because of the number of species (6–8) involved in these electrochemical reactions, and the rapid rates of the chemical steps. Feldberg's fast quasi-explicit finite difference method (FQEFD) [33] provided a useful approach to these simulations, since it is efficient for such stiff problems. We found that under these conditions the FQEFD method was up to 40 times faster than the explicit finite difference (EFD) method, with use of exponential expanding grids in both.

The effect of v and concentration on the first peak current, the peak potential and the potential difference between the peak current and the half-peak current, are sensitive to the different coupling mechanisms and can be used to discriminate among them. Typical simulated cyclic voltammograms for the different coupling pathways with the same scan rate (0.1 V s^{-1}) and other kinetic parameters are given in Fig. 10 and the results are summarized in Table 2. These simulations assumed that all heterogeneous electron transfer steps are rapid with $\alpha = 0.5$. Thus, k_s values of 1.0 cm s^{-1} were used in the results in Figs. 10 and 11. Larger k_s values in the simulations gave identical results.

The first anodic wave should be most useful for discrimination among the different possibilities, because it reflects the contributions of the following chemical steps. For example, the redox potentials of the dimers, benzidine and ADPA, are more negative than that of aniline; thus, they are oxidized at the first wave and contribute to I_{pa}. The current function of the first anodic peak in the R–R mechanism is larger than those for the other mechanisms. The peak potential shifts toward positive values by about 20 mV per decade of scan rate for (1) R–R, but 30 mV in the others in the slow scan rate region (KP region, pure kinetic region [31]). The potential difference between the first anodic peak and its half peak is about 40 mV in (1), but 60 mV in the others in this KP region. This criterion is even more important in the present study, because only the working curve for this criterion (E_p vs. v) can be clearly divided into three zones: KP, KO (where both diffusional and kinetic contributions are present) and DP [26]. For the other two criteria, the zone boundaries are not as clear.

In addition to these three criteria, the shape of the voltammogram is also important. If two dimers, benzidine and ADPA, are formed by different coupling pathways, but with the fixed rate constants of the two coupling routes, the shape of the voltammogram is completely different. Over 1200 voltammograms with different homogeneous reaction rate constants for the two mechanisms were simulated; a few typical voltammograms are shown in Figs. 10(b)–10(d). The ratio of the cathodic peak currents for the two species to the first anodic peak current is unique. It depends strongly on the coupling routes and their rates.

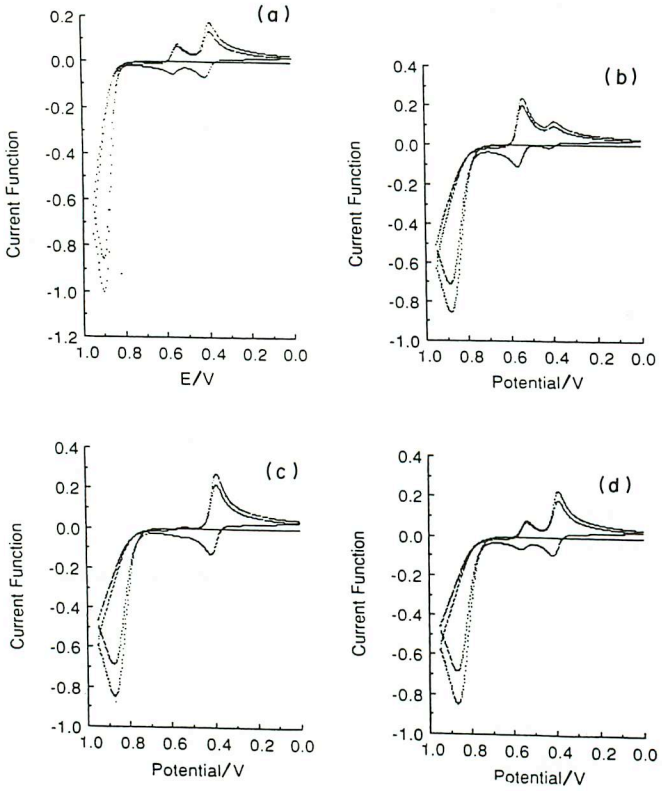

Fig. 10. Simulated cyclic voltammograms based on four different mechanisms: (a) R–R; (b) R–P1; (c) R–P1′; (d) R–P2. Other conditions were $k_2 = 10^7$ M^{-1} s^{-1}, $k_1 : k_2 = 4:10$, $k_s = 1.0$ cm s^{-1}, $\alpha = 0.5$, $D = 1.5 \times 10^{-6}$ cm^2 s^{-1}, $v = 0.1$ V s^{-1}.

TABLE 2

Simulated voltammetric results [a]

	Current function	First peak potential vs. $E^{o\prime}$/mV	$E_p - E_{p/2}$ /mV	Ratio of the first I_{pa} and the first I_{pc1}, I_{pc2}
R–R	1.0330	−48.4	39.3	11:0.64:1
R–P1	0.8562	−76.0	58.2	35.6:8.8:1
R–P1′	0.8536	−88.8	58.0	3.79:0.083:1
R–P2	0.8536	−92.7	58.1	5.74:0.58:1

[a] In simulation, $k_s = 1.0$ cm s^{-1}, $\alpha = 0.5$, $D = 1.5 \times 10^{-6}$ cm^2 s^{-1}, $k_1 = 4 \times 10^6$ M^{-1} s^{-1}, $k_2 = 1 \times 10^7$ M^{-1} s^{-1}.

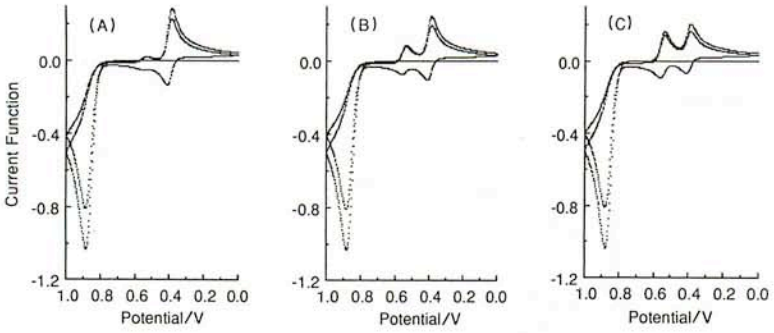

Fig. 11. Simulated cyclic voltammograms based on R–R mechanism with different ratios of $k_1 : k_2$: (A) 1:10, (B) 4:10, (C) 10:10. Other conditions were $k_2 = 10^7$ M^{-1} s^{-1}, $k_s = 1.0$ cm s^{-1}, $\alpha = 0.5$, $D = 1.5 \times 10^{-6}$ cm^2 s^{-1}, $v = 0.1$ V s^{-1}.

A comparison of the simulation data with the experimental voltammetric results at a GC electrode leads to the conclusion that both benzidine and ADPA are formed exclusively by R–R coupling in the initial stage of polymerization of aniline. To estimate the rate constants for these two R–R couplings, another comparison of the simulation data was needed. Figure 11 shows the simulated cyclic voltammograms with different ratios of k_1 to k_2, where k_1 is the rate constant for R–R coupling to produce benzidine and k_2 is the rate constant for R–R coupling to produce ADPA. The rate constant of dimerization for ADPA is of the order 10^7 M^{-1} s^{-1} and is about 2.5 times faster than that for benzidine.

Unfortunately, GC ultramicroelectrodes were not available, so it was impossible to change the scan rate by 5–6 orders of magnitude to obtain a more complete series of data points for fitting to the working curve to determine the rate constant more precisely. However, the discrimination of R–R and R–P could be seen even at slow scan rates.

Observation of the reduction wave of aniline radical cation in MeCN solution

The radical cation of aniline is expected to be the least stable of the aromatic amines. No spectroscopic or electrochemical experimental evidence for the existence of aniline radical cations has ever been reported. The rate constant for the coupling reaction was estimated to be above 10^7 M^{-1} s^{-1}, leading to a lifetime of approximately 2 ms at a concentration of 5×10^{-5} M.

In non-aqueous solutions, polyaniline films are also formed upon the oxidation of aniline [34–37]. The mechanism of oxidation of aniline and polymer growth in this case, however, has not been fully elucidated. We intended to employ fast scan cyclic voltammetry (above 50 000 V s^{-1}) to observe the reduction wave for the aniline radical cations, but this was unsuccessful. The radical cation coupling reaction in aqueous solution is a second-order reaction. In the present case, when the concentration of aniline is below 5 mM, the current signal for the reduction of

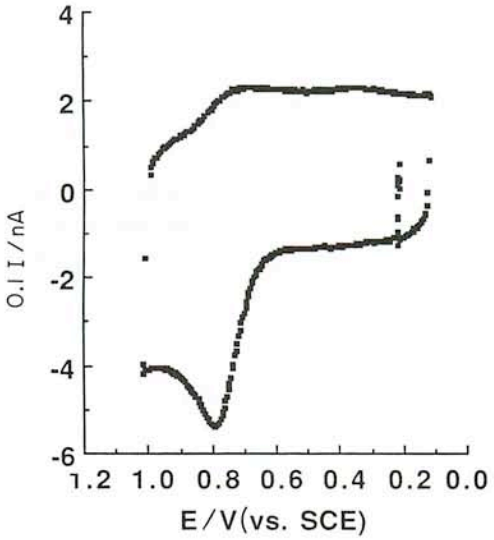

Fig. 12. Cyclic voltammogram of 50 μM aniline in 0.1 M $TBAPF_6$–MeCN solution with 25 μm diameter platinum disk at a scan rate of 200 V s^{-1}.

radical cations at scan rates above 5 000 V s^{-1} was not large enough to measure with a carbon fiber microelectrode with background subtraction. Alternatively, if the concentration was increased above 5 mM, even faster scan rates would be required. However, by employing a very low concentration of aniline, it was possible to observe a back reduction wave at moderate scan rates. Figure 12 is the voltammogram obtained with 0.05 mM aniline at $v = 200$ V s^{-1}, without background subtraction. This voltammogram, for the first time, shows a small reduction wave of aniline radical cation and is consistent with a coupling rate constant in acetonitrile solution of about 10^8 M^{-1} s^{-1}.

DISCUSSION

Recently, there has been some controversy over the interpretation of the "middle" peaks in the cyclic voltammograms. Kitani et al. [38] interpreted these peaks as resulting mostly from the redox reaction of benzoquinone. Stilwell and Park [11] suggested that these peaks might be the result of redox reactions of benzoquinone, *p*-aminophenol, PPD(*N*-phenyl-*p*-phenylenediamine), and ADPA. Genies et al. [17], however, proposed that the middle peak is the result of phenazine insertion.

Our voltammetric and simulation results favor the mechanisms proposed by Kitani et al. and Stilwell and Park. Moreover, the identification of the middle peak depends upon the time scale and aniline concentration. When a high aniline concentration is used at slow scan rates, the middle peaks can be interpreted as

the result of the redox reactions of *p*-hydroxydiphenylamine and ADPA in the early stages, but that of benzoquinone and *p*-aminophenol later. Alternatively, at fast scan rates, oxidative hydrolysis is suppressed and the middle peak is a result of the redox reaction of ADPA. When a lower aniline concentration is used, only ADPA is the source of the middle peak. Overall, ADPA is the dominant intermediate with the fastest reaction kinetics.

Note that in the presence of a small amount of benzidine in the aniline solution, the oxidation of benzidine can also result in the formation and growth of polymer, even with the potential controlled before the oxidation of aniline [13]. The middle peak still appeared in this case, which suggests that this peak may also result from a small oligomer with the diphenylamine structure. For example,

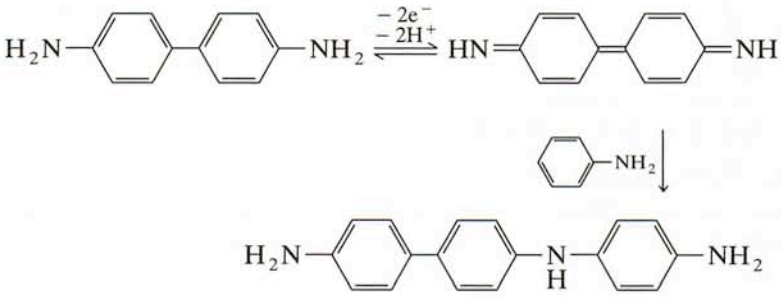

This trimer has a

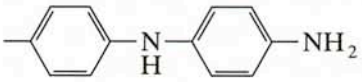

unit, which may have a redox potential similar to ADPA. Therefore, the middle peak could either be that of ADPA or of a small oligomer with an ADPA unit.

Another similar experiment was carried out with phenazine in the aniline–H_2SO_4 solution. A one-electron transfer reversible wave for the redox reaction of phenazine was observed at a potential of -0.3 V vs. SMSE (Fig. 13), which is more negative than the middle peak and in the polaron redox potential region. However, potential cycling of phenazine did not lead to the formation of polymer without the oxidation of aniline. When the switching potential was shifted to values more positive than that for aniline oxidation, a bright blue film formed, which was probably a copolymer of aniline and phenazine.

Stilwell and Park [11] pointed out that the polyaniline growth followed an autocatalytic mechanism and the rate constant was first order in aniline concentration in a reaction of the R–P type. We have found that increased aniline concentrations (greater than 5 mM) will lead to changes in the voltammetric characteristics even with a GC electrode used in the cyclic voltammetry measurements. The potential difference of the first peak and half peak increased to 60 mV and the component of the first peak current in the ratio of the three peaks increased as well. An explanation of this might be that as the concentration of aniline increases, the kinetics of the autocatalytic reaction play a more important

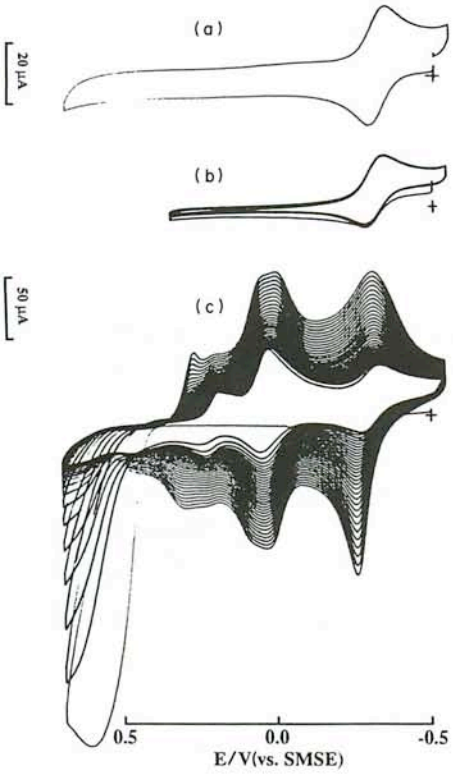

Fig. 13. Cyclic voltammograms of 1.55 mM phenazine in 1 M H_2SO_4 with 3 mm diameter glassy carbon electrode at a scan rate of 0.1 V s^{-1}, (a) in the absence of aniline, (b) 15th cycle in the presence of 10 mM aniline, and (c) in the presence of 10 mM aniline cycling over aniline oxidation wave.

role, and therefore the shape of the first peak is affected. The peak current will be enhanced because of contributions not only from the oxidation of aniline, benzidine, and ADPA, but also from trimers and oligomers. If the trimers and other oligomers have a significant contribution to the first peak current, then the autocatalytic reaction kinetics will affect the $E_p - E_{p/2}$ value. Such an interpretation might also be applied to the results reported by Gao et al. in the case when the aniline concentration increased [32]. Other reactions, e.g. cross-linking reactions, may also be involved in the polymer growth, but their kinetics do not appear sufficiently fast to be important in the initial stage of polymerization.

CONCLUSIONS

The initial stage of electropolymerization of aniline in acidic aqueous solution was studied by cyclic voltammetry with different scan rates and different electrodes, SEM and STM, and digital simulation. ADPA, a dimer of aniline, is a

dominant intermediate in the earlier stage of polymerization, i.e. the dimerization leading to the formation of ADPA has the fastest reaction rate. Benzidine is a minor intermediate. The middle peaks actually reflect the occurrence of oxidative hydrolysis and degradation reactions. At a platinum electrode and slow scan rates, the middle peaks result from a redox reaction of (1) *p*-hydroxydiphenylamine and ADPA in the early stages, and (2) benzoquinone and *p*-aminophenol in the later stages. However, at fast scan rates, oxidative hydrolysis can be suppressed and the middle peak is only a result of a redox reaction of ADPA or small oligomers with an ADPA unit. The electropolymerization of aniline can be kinetically controlled by changing scan rates to minimize the contribution of degradation reactions. SEM and STM images of polyaniline films formed at fast scan rates show them to be more uniform, compact, and of a regular structure. No microfiber structure was observed with these thin films.

Further studies with a GC electrode at low concentrations of aniline solutions, combined with digital simulation, indicate that both intermediates, benzidine and ADPA, are formed through a radical-cation–radical-cation coupling pathway. The resulting mechanisms of oxidation of aniline, dimerization, and polymerization are proposed in Scheme 1. The reduction wave of the aniline radical cation in MeCN solution was observed for the first time. The rate constant of the chemical reaction between radical cations is estimated to be about 10^8 M^{-1} s^{-1}.

ACKNOWLEDGMENTS

The support of this research by the National Science Foundation (CHE8901450) is gratefully acknowledged. We thank Y.-T. Kim for obtaining the STM images.

APPENDIX A

In digital simulations, several assumptions have been made to simplify the problem: (i) the kinetic parameters, k_s and α, in all electron transfer steps are the same; (ii) the diffusion coefficients for all species are the same; (iii) no cross reactions or disproportionation reactions are considered; (iv) in the mechanisms with R–P type coupling pathways, another one-electron transfer from a redox reaction of the product of radical–parent coupling is necessary to keep n_{app} the same as in the R–R coupling pathway. The four mechanisms to be considered could written as:

(1) R–R

$A - e^- \rightleftarrows B$ at E_1°, k_s, α

$2B \rightarrow C$ k_1

$C - 2e^- \rightleftarrows D$ at E_2°, k_s, α

$2B \rightarrow E$ k_2

$E - 2e^- \rightleftarrows F$ at E_3°, k_s, α

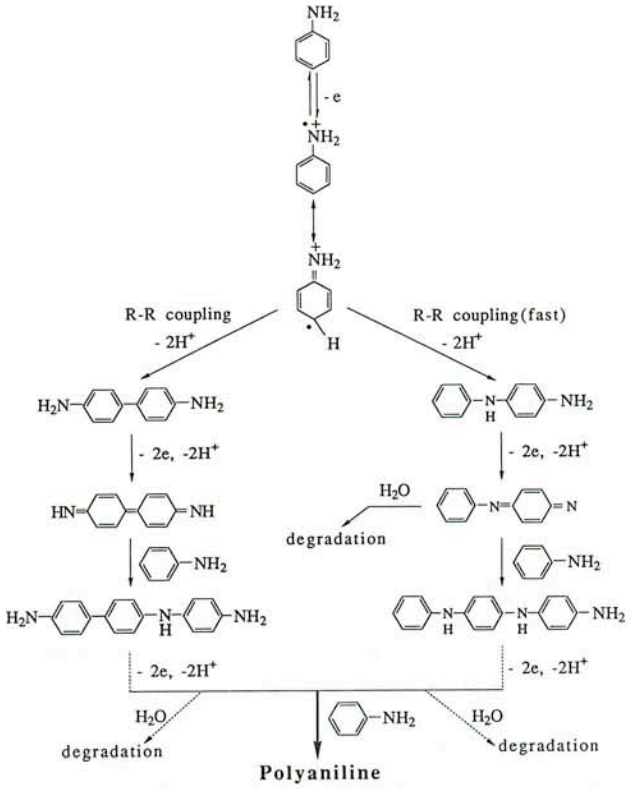

Scheme 1.

(2) R–P1

$A - e^- \rightleftarrows B$ at E_1°, k_s, α

$A + B \rightarrow G$ k_1

$G - e^- \rightleftarrows C$ at E_4°, k_s, α

$C - 2e^- \rightleftarrows D$ at E_2°, k_s, α

$2B \rightarrow E$ k_2

$E - 2e^- \rightleftarrows F$ at E_3°, k_s, α

(3) R–P1′

$A - e^- \rightleftarrows B$ at E_1°, k_s, α

$2B \rightarrow C$ k_1

$C - 2e^- \rightleftarrows D$ at E_2°, k_s, α

$A + B \rightarrow H \quad k_2$

$H - e^- \rightleftarrows E \quad$ at E_4°, k_s, α

$E - 2e^- \rightleftarrows F \quad$ at E_3°, k_s, α

(4) R–P2

$A - e^- \rightleftarrows B \quad$ at E_1°, k_s, α

$A + B \rightarrow G \quad k_1$

$G - e^- \rightleftarrows C \quad$ at E_4°, k_s, α

$C - 2e^- \rightleftarrows D \quad$ at E_2°, k_s, α

$A + B \rightarrow H \quad k_2$

$H - e^- \rightleftarrows E \quad$ at E_4°, k_s, α

$E - 2e^- \rightleftarrows F \quad$ at E_3°, k_s, α

where C and E represent the dimers benzidine and ADPA respectively.

The fast kinetics involved in these processes, i.e. the large rate constants of homogeneous chemical reactions, have made the simulations potentially demanding of large computing times. These problems can be circumvented in many ways, such as adopting the heterogeneous equivalent method, which is very efficient [39], but only valid in a limited kinetic regime. A general, attractive approach is the FQEFD method [33] which is applicable to any stiff system of complicated reaction mechanisms and fast kinetics, such as square-scheme reactions [40]. This approach involves calculating the concentration profile by solving $(n \times n)$ linear equations (assuming n species are involved in the system). Gauss–Jordan elimination is a simple method for achieving this.

As mentioned above, $k_2/k_1 = 2.5$; therefore, $k_2 = 10^7\ M^{-1}\ s^{-1}$, $k_1 = 4 \times 10^6\ M^{-1}\ s^{-1}$ were used in the simulation. For heterogeneous kinetics, $k_s = 1.0\ cm\ s^{-1}$, $\alpha = 0.5$ were assumed. The dimensionless parameter $\lambda = (k_1 + k_2)cRT/Fv$ was the kinetic variable. Three types of working curves are presented here.

Figure A1 is the variation of current function vs. log λ. A large difference is observed in the first oxidation peak current in the KP zone. Even though the n_{app} value in all of the four mechanisms is the same, the current functions in the case of R–R are about 20% higher than those in other cases, which is similar to that reported previously [26]. However, whenever an R–P type reaction is involved in the mechanisms, the behavior for the variation of the current function, as well as E_p–$E_{p/2}$, vs. log λ is almost identical. Furthermore, for R–P1, R–P1′ and R–P2, the contributions of the electron transfer steps after the oxidation to the total current were smaller than predicted from the overall n_{app} values. In the present simulation, $k_{R-P} : k_{R-R} = 4 : 10$. Note that even if the ratio $k_{R-P} : k_{R-R}$ was changed to 1 : 10, the variation of current function vs. log λ would not be significantly affected. An increase in the current functions in the KP zone was observed

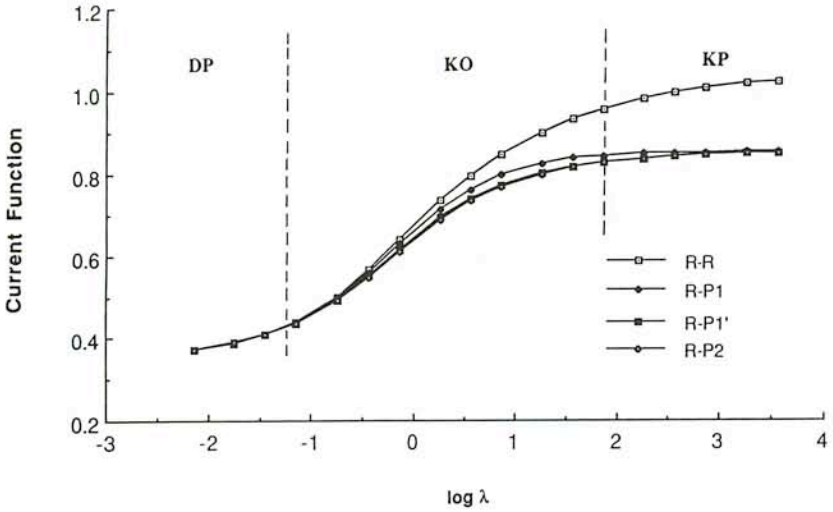

Fig. A1. Simulation of variation of the current function of the first peak vs. log λ, where $k_1 = 4\times10^6$ M^{-1} s^{-1}, $k_2 = 10^7$ M^{-1} s^{-1}, $k_s = 1.0$ cm s^{-1}, $\alpha = 0.5$, $D = 1.5\times10^{-6}$ cm^2 s^{-1}.

up to $k_{R-P} : k_{R-R} = 1:100$. This suggests that the R–P type of coupling had a dominant effect on the overall electrochemical behavior.

Figure A2 shows the variation of the potential shift of the first peak with respect to its formal potential vs. log λ. This indicates that the first peak potentials in all

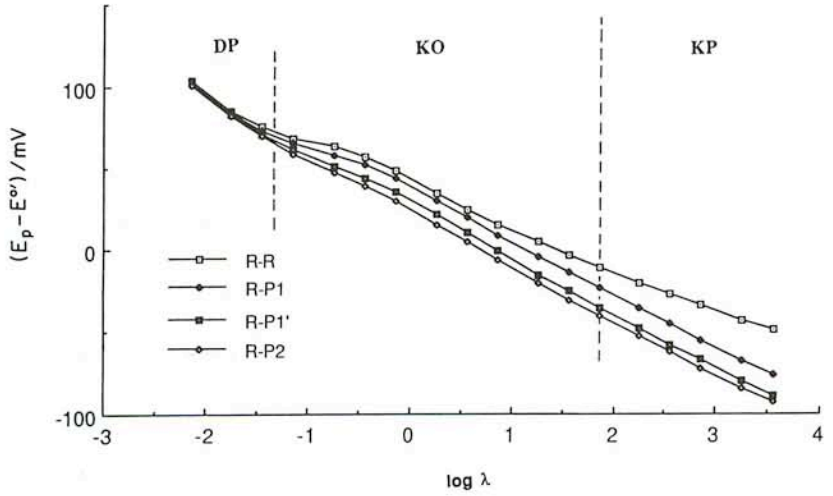

Fig. A2. Simulation of variation of the first peak potential shift vs. log λ. Other conditions are the same as in Fig. A1.

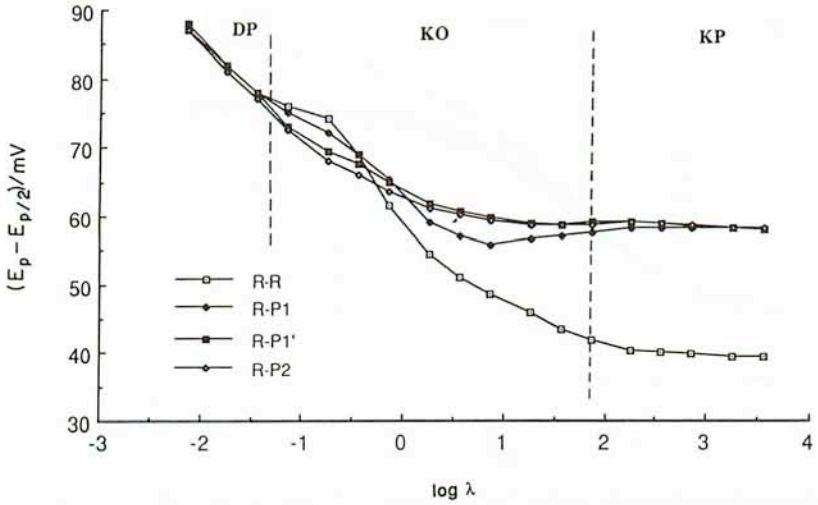

Fig. A3. Simulation of variation of $(E_p - E_{p/2})$ vs. log λ. Other conditions are the same as in Fig. A1.

four mechanisms shift in the negative direction for oxidations in the slow scan rate region, i.e. KP zone. However, the slopes, $\partial(E_p)/\partial(\log \lambda)$ are different. A negative shift of about 20 mV is observed for a ten-fold increase in λ for scheme (1) whereas a slope of about 30 mV per ten-fold increase in λ is found for schemes (2), (3), and (4). The plots of (2), (3), and (4) are almost parallel to each other, but the negative potential shift of (4) is the most dominant. It is difficult to deduce KP and KO zones in this figure.

A pronounced difference between mechanisms, similar to that in Fig. A1, is observed in Fig. A3. The half-peak potential separation $(E_p - E_{p/2})$ in the KP zone is 40 mV only for (1). For the other cases, the half-peak potential separation in the KP zone is 58 mV. Therefore, this is a very useful criterion for distinguishing R–R coupling from any kind of R–P type coupling.

From the above three working curves, it is possible to distinguish R–R from R–P type couplings. It is hard to discriminate among schemes (2), (3) and (4). The variations in all three figures for (2), (3), and (4) are very similar, if not identical. In this case, an analysis of the first peak fails to provide enough information about relative contributions of the two dimerization paths and an additional analysis of the ratio of the three peaks is necessary.

Since two chemical reactions are involved in all four mechanisms, the kinetic variables are $\lambda_1 = k_1 cRT/Fv$ and $\lambda_2 = k_2 cRT/Fv$ respectively. The variation of λ_1 and λ_2 independently can provide a whole spectrum of general electrochemical responses for this situation. Thus, three-dimensional working curves have been developed [41].

REFERENCES

1 A.F. Diaz and J.A. Logan, J. Electroanal. Chem., 111 (1980) 111.
2 D.M. Mohilner, R.N. Adams and W.J. Argersinger, J. Am. Chem. Soc., 84 (1962) 3618.
3 R. DeSurville, M. Josefewicz, L-T. Yu, J. Perichon and R. Buvet, Electrochim. Acta, 13 (1968) 1451.
4 R.N. Adams, Electrochemistry at Solid Electrodes, Marcel Dekker, New York, 1969.
5 R.F. Nelson, in A. Weissberger (Ed.), Techniques of Chemistry, Vol. 5.
N.L. Weinberg (Ed.), Technique of Electroorganic Synthesis, Part 1, Wiley, New York, 1974.
6 R.C. Reed and R.M. Weightman, in A.J. Bard (Ed.), Encyclopedia of Electrochemistry of the Elements, Organic Section, Vol. XV, Marcel Dekker, New York, 1984.
7 A.G. MacDiarmid, J.-C. Chiang, M. Halpern, W.-S. Huang, S.-L. Mu, N.L.D. Somasiri, W. Wu and S.I. Yaniger, Mol. Cryst. Liq. Cryst., 121 (1985) 173.
8 A.F. Diaz and J. Bargon, in T.A. Skotheim (Ed.), Handbook of Conducting Polymers, Vol. 1, Marcel Dekker, New York, 1986.
9 A.G. MacDiarmid and A. Epstein, J. Chem. Soc., Faraday Trans., 5 (1989) 1.
10 E.M. Genies, A. Boyle, M. Lapkowski and C. Tsintavis, Synth. Met., 36 (1990) 182.
11 D.E. Stilwell and S.-M. Park, J. Electrochem. Soc., 135 (1988) 2254, 2497.
12 Y.-B. Shim and S.-M. Park, Synth. Met., 29 (1989) E169.
13 Y.-B. Shim, M.-S. Won and S.-M. Park, J. Electrochem. Soc., 137 (1990) 538.
14 G. Zotti, S. Cattarin and N. Comisso, J. Electroanal. Chem., 235 (1987) 259.
15 G. Zotti, S. Cattarin and N. Comisso, J. Electroanal. Chem., 239 (1988) 387.
16 E.M. Genies and M. Lapkowski, J. Electroanal. Chem., 236 (1987) 189.
17 E.M. Genies, M. Lapkowski and J.F. Penneau, J. Electroanal. Chem., 249 (1988) 97.
18 E.M. Genies, J.F. Penneau, M. Lapkowski and A. Boyle, J. Electroanal. Chem., 269 (1989) 63.
19 J.C. Chiang and A.G. MacDiarmid, Synth. Met., 13 (1988) 193.
20 W.-S. Huang, B.D. Humphrey and A.G. MacDiarmid, J. Chem. Soc., Faraday. Trans. 1, 82 (1986) 2385.
21 A.G. MacDiarmid, J.-C. Chiang, A.F. Richter and A.J. Epstein, Synth. Met., 18 (1987) 285.
22 G.E. Wnek, Synth. Met., 15 (1986) 213.
23 A.J. Epstein, J.M. Ginder, F. Zuo, R.W. Bigelow, H.-S. Woo, D.B. Tanner, A.F. Richter, W.-S. Huang and A.G. MacDiarmid, Synth. Met., 18 (1987) 303.
24 A.J. Epstein, J.M. Ginder, F. Zuo, H.-S. Woo, D.B. Tanner, A.F. Richter, M. Angelopoulos, W.-S. Huang and A.G. MacDiarmid, Synth. Met., 21 (1987) 63.
25 P. Chandrasekhar and R.W. Gumbs, J. Electrochem. Soc., 138 (1991) 1337.
26 H. Yang and A.J. Bard, J. Electroanal. Chem., 306 (1991) 87.
27 H. Yang, D.O. Wipf and A.J. Bard, J. Electroanal. Chem., in press.
28 Y.-T. Kim, H. Yang and A.J. Bard, J. Electrochem. Soc., 138 (1991) L71.
29 R.L. Hand and R.F. Nelson, J. Am. Chem. Soc., 96 (1974) 850.
30 S. Fletcher, C.S. Halliday, D. Gates, M. Westcott, T. Lwin and G. Nelson, J. Electroanal. Chem., 159 (1983) 267.
31 A.J. Bard and L.R. Faulkner, Electrochemical Methods, Wiley, New York, 1980.
32 P. Gao, D. Gosztola and M.J. Weaver, J. Phys. Chem., 93 (1989) 3753.
33 S.W. Feldberg, J. Electroanal. Chem., 290 (1990) 49.
34 M.C. Miras, C. Barbero, R. Kotz and O. Haas, J. Electrochem. Soc., 138 (1991) 335.
35 T. Ohsaka, Y. Ohnuki, N. Oyama, G. Katagiri and K. Kamisako, J. Electroanal. Chem., 161 (1984) 399.
36 T. Osaka, S. Ogano, K. Naoi and N. Oyama, J. Electrochem. Soc., 136 (1989) 306.
37 T. Osaka, T. Nakajima, K. Naoi and B.B. Owens, J. Electrochem. Soc., 137 (1990) 2139.
38 A. Kitani, M. Kaya and K. Sasaki, J. Electrochem. Soc., 133 (1986) 1069.
39 I. Ruzic and S.W. Feldberg, J. Electroanal. Chem., 50 (1974) 153.
40 S.A. Lerke, D.H. Evans and S.W. Feldberg, J. Electroanal. Chem., 296 (1990) 299.
41 H. Yang, Ph.D. Dissertation, The University of Texas at Austin, 1991, Chapter 7.